Probabilistic slope stability analysis: A novel distribution for soils exhibiting highly variable spatial properties

Vincent Renaud, Marwan Al Heib

Probabilistic slope stability analysis: a novel distribution for soils exhibiting highly variable spatial properties

Vincent Renaud [a*] and Marwan Al Heib [a]

[a] Institut national de l'environnement industriel et des risques (Ineris)- ARTEM, 54042 Nancy- France

* Corresponding author: vincent.renaud@ineris.fr; Tel.: +0033-3-5440-6632, ORCID ID: 0000-0003-0759-9995

Abstract:

Slope stability calculation depends on the soil properties (cohesion and the friction angle) of the soil. Heterogeneous terrains are frequently observed in civil and mining projects where the properties are highly spatially variable. Based on a real data from case studies, this paper presents a probabilistic analysis of the slope stability of highly heterogeneous terrains with a very high coefficient of variation (COV) of the cohesion distribution. The existing deterministic and probabilistic approaches for calculating slope stability lack the capability to effectively consider the significant heterogeneity present in the terrain The objective of the paper is to develop a new bounded interval distribution having a COV that is as high (> 150%) as the COV of the cohesion distribution The results obtained with this new distribution are compared to 4 other semi-infinite distributions. To consider the correlation between cohesion and the friction angle, a specific formulation was developed to generate friction angles varying between fixed minimum and maximum limits and having the desired correlation coefficient, mean, and standard deviation. The new cohesion and friction angle distributions were incorporated and tested in a probabilistic numerical model. The new distribution can presently be applied to geotechnical studies for terrains and heterogenous materials with properties exhibiting high spatial variability.

Keywords: Monte-Carlo simulation, slope stability, probability distribution, heterogeneous materials.

1 Introduction and objective

The slope instability is a major problem in civil, mining, and geohazard engineering. The inherent spatial variability of geo-material properties influences material behaviour and geo-structural response [1,2]. Analytical and numerical approaches are generally used to assess their local and global stability and to calculate a safety factor. In fact, using a deterministic approach that does not account for spatial variability can sometimes cause slope failure even when the "deterministic" factor of safety (FoS) is greater than 1.0. Spatial variability is particularly important since the response of the terrain depends on its geomechanical properties, with failure often initiating and spreading from the weakest areas of the massif [3]. Probabilistic approaches provide a more robust assessment, delivering a comprehensive response articulated in terms of reliability and the probability of failure [4,5].

Probabilistic approaches of slope stability problems are not new, and have been used since the 1970s [6,7,8,9], mainly by combining limit equilibrium methods with various probabilistic approaches [10]. Those approaches have included the Monte Carlo Simulation (MCS) method [11,12,13,14,15]. The MCS method calculates the probability of slope failure based on the assumption of the probability density function (pdf) of the random input variables [12].

The advantages of MCS method are: standard errors in the results are very easy to determine, the convergence speed is independent of the magnitude of the random variables and the complexity of the performance function is not related to the simulation procedure. The disadvantage of the MCS is that the number of simulations and the computation time increase considerably with the reduction of

the probability of failure. MCS is also used in numerical calculations, in particular to vary the properties of the terrain (plastic and/or elastic), of rock joints [16], or of bimrocks [17]. Most often, it is the values of the parameters under consideration that are distributed, but with the RS-DEM method (the Random Set Discrete Element Method, the theory of which is attributed to Kendal [18]) only the intervals of the input parameters are considered. The finite element method (FEM [3], Random FEM [19], stochastic finite element [20]), finite difference method (FDM [21,22,23]) and discrete element method (DEM, [24] have been adopted more recently as alternatives to the limit equilibrium method. This paper provides a new distribution that can represent data with high spatial variability, using example data (cohesion and friction angle) generated for use with the combined MCS and FDM methods.

The paper specifically addresses the case of a mining deposit structure resulting from the excavation of mines and tunnels. A mining deposit consists of high heterogeneity materials [25,26,27,28,29,30]. This heterogeneity – also referred to as "natural variability" - is due to the nature of the different constituents, their granulometry, the method of construction, the reaction with runoff, consolidation, etc. This level of heterogeneity justifies considering a spatial distribution of the mechanical properties instead of a vertical gradient, as is often the case for consolidated homogeneous soil layers [30]. The objective of the paper is to develop a suitable distribution for the cohesion with high dispersion, and to then apply it to real cases.

2 Distribution of widely dispersed data

Slope stability is a major problem [31,32,33] in geotechnical engineering. It depends, among other things, on the nature of the soil and its heterogeneity. The paper discusses the distribution of geomechanical properties affecting the global stability of the slope of mining deposits.

The stability calculation is based on the factor of safety value (FoS). Analytically, it depends on the ratio of the driving forces and those related to the shear strength of the geomaterial. The shear strength is expressed in terms of a failure criterion such as Mohr-Coulomb criterion. This criterion is described by a cohesion C and a friction angle ϕ. Because these two parameters vary spatially, they are random variables. Additionally, the coefficient of variation (COV) is a dimensionless parameter that characterises the heterogeneity of the soil [34]. The cohesion and friction angle data of a mining deposit in Greece - Soulou [35] only show that the coefficient of variation (COV) of the measured cohesions is very high (COV = 143%, Table 1). The literature on heterogeneous soils [30, 34, 36, 37, 38] reports a greater variability in the cohesion parameter (clay soil = 75% < COV < 186% = fly ash) than in the angle of friction (sand = 7% < COV < 72% = soils with high clay content).

27 samples	cohesion	friction angle	variation interval
mean	μ_C = 14.2 kPa	μ_ϕ = 25.9°	C: [0 kPa; 72 kPa]
standard deviation	σ_C = 20.3 kPa	σ_ϕ = 7.8°	ϕ: [8°; 39°]
COV = σ/μ	COV = 143 %	COV = 28 %	

Table 1 : Statistical parameters of cohesion and friction angle measured in laboratory tests (27): case of a mining deposit [35]

For the case study presented in Table 1, it is therefore impossible to obtain a good statistical representation of cohesion measurements with a conventionally adopted normal distribution. The parameters C and ϕ, like most mechanical parameters, are positive data. To ensure that 99.8% of the data is positive under a normal distribution, it is essential that μ-3$\sigma \geq 0$, corresponding to COV $\leq$ 33%. The distribution of the friction angle can be effectively approximated by a normal distribution. This is evident as the coefficient of variation (COV) is 28 %, which corresponds to μ-3.57 σ = 0, and which, in turn, represents 99.98% of positive data. The friction angle was measured in the interval [8°; 39°] which corresponds to: [μ_ϕ - 2.32 σ_ϕ; μ_ϕ + 1.68 σ_ϕ]. This means that 99% of the data below μ_ϕ will be correctly distributed by a normal distribution whereas only 95% will be for those above μ_ϕ. To overcome this

drawback, data censoring (if $X > X_{max}$ then $X=X_{max}$ and if $X < X_{min}$ then $X=X_{min}$) can be performed during the random generation of the friction angles, as shown in Fig. 1, the interval-censoring concerns just a few data items and does not significantly disrupt the normal distribution, which could therefore be adopted for the friction angle.

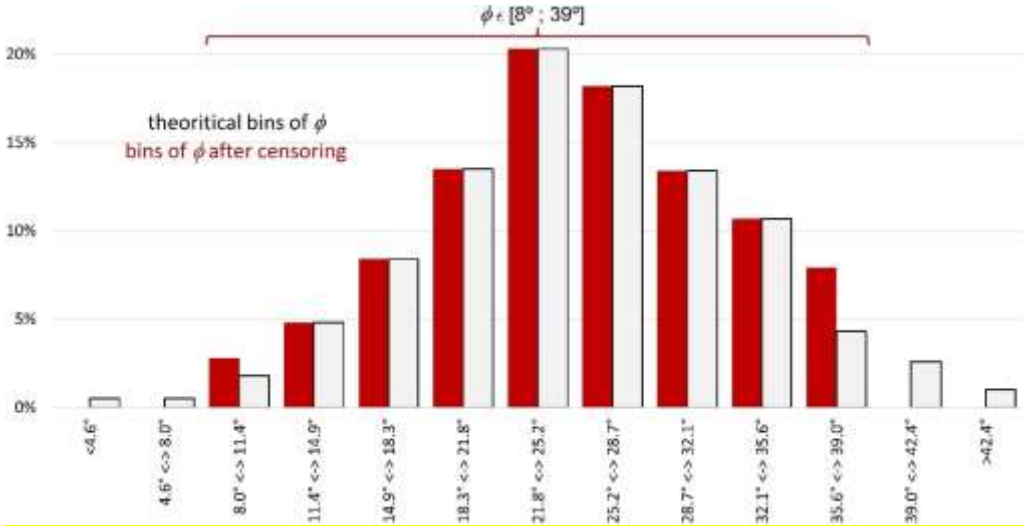

Fig. 1 : Normal distribution of the friction angle, before and after interval-censoring

The analysis of cohesion measurements [35] reveals a substantial difference between the median value (6.6 kPa) and the mean value (14.2 kPa), because 11 out of the 27 measurements are nearly zero. This indicates a skewed distribution with an extended right-hand tail, emphasizing the necessity of considering this information when the skewness coefficient is unknown. Using the definition of the non-parametric skewness coefficient, the skewness in this case turns out to be notably pronounced because $\frac{\mu - median}{\sigma} = 0.37 > 0.2$ [39].

As of the current state of knowledge, there have been no probabilistic studies specifically addressing highly heterogeneous geomaterials (COV > 100%). Among the many existing continuous distributions, relatively few can effectively reproduce data with a very high COV. In fact, to effectively represent the distribution of cohesion (a positively skewed variable with significant variability), there are two possibilities among the continuous distributions: distributions defined on a bounded interval or distributions defined on a semi-infinite interval. A priori, because cohesion is a positive variable belonging to a bounded interval, the natural choice should be the first possibility. This would mean ignoring the complexity of the distribution and/or density functions, which may prevent the consideration of certain distributions that are very difficult to implement in software.

This work first presents the most used distributions in geomechanics and their results. It then describes the development of a new distribution capable of accounting for these high levels of dispersion.

2.1 Continuous distributions defined on a bounded interval

In the literature, two distributions defined on a bounded interval [0; C_{max}] can reproduce data with high COV: generalized ARGUS [40] and Beta:

ARGUS: Probability density function: $$\mathrm{pdf} = \left(\frac{\chi}{C_{\max}}\right)^{2(p+1)} \frac{(C_{\max}-x)(x(2C_{\max}-x))^{p}}{2^{p}\left(\Gamma(p+1)-\Gamma\left(p+1,\frac{\chi^{2}}{2}\right)\right)} \mathrm{e}^{-\frac{x}{2}\left(\frac{\chi}{C_{\max}}\right)^{2}(2C_{\max}-x)} \quad (1)$$

Cumulative Distribution Function: $$\mathrm{CDF}=\frac{\Gamma\left(p+1,\frac{\chi^2}{2}\left(1-\frac{x^2}{C_{\max}^2}\right)\right)-\Gamma\left(p+1,\frac{\chi^2}{2}\right)}{\Gamma(p+1)-\Gamma\left(p+1,\frac{\chi^2}{2}\right)} \quad (2)$$

where χ (>0) and p (>-1) are the shape parameters (curvature and power) and $\Gamma(a,z)$ is the upper incomplete Gamma function ($\Gamma(a,z)=\int_z^\infty t^{a-1}e^{-t}dt$). This distribution has been adjusted for positive skewness by transforming the variable $x \rightarrow C_{\max} - x$, as opposed to the original formula [40].

Beta (for $C_{\min} \le x \le C_{\max}$): $$\mathrm{pdf}=\frac{\Gamma(\alpha+\beta)}{\Gamma(\alpha)\Gamma(\beta)(C_{\max}-C_{\min})^{\alpha+\beta-1}}(x-C_{\min})^{\alpha-1}(C_{\max}-x)^{\beta-1} \quad (3)$$

$$\mathrm{CDF}=\int \mathrm{pdf}\,dx=\frac{\Gamma(\alpha+\beta)}{\Gamma(\alpha)\Gamma(\beta)}\mathrm{B}_{\frac{x-C_{\min}}{C_{\max}-C_{\min}}}(\alpha,\beta) \quad (4)$$

where $\mathrm{B}_z(\alpha,\beta)$ is the incomplete Beta function ($\mathrm{B}_z(\alpha,\beta)=\int_0^z t^{\alpha-1}(1-t)^{\beta-1}dt$).

The Beta distribution has several advantages over the ARGUS distribution: the density function is easily calculated (the Gamma function is easily programmable), the mean and standard deviation have analytically invertible forms, and the cohesions can be represented with a COV equal to or below 202%. Knowing the mean and standard deviation of the data, it is easy to determine the shape parameters α and β:

$$\alpha=\frac{(\mu-C_{\min})\left(\mu(C_{\max}+C_{\min})-C_{\max}C_{\min}-\sigma^2-\mu^2\right)}{(C_{\max}-C_{\min})\sigma^2} \quad (5)$$

and $$\beta=\frac{(C_{\max}-\mu)\left(\mu(C_{\max}+C_{\min})-C_{\max}C_{\min}-\sigma^2-\mu^2\right)}{(C_{\max}-C_{\min})\sigma^2} \quad (6)$$

The density function remains positive if $\alpha > 0$ or $\beta > 0$., i.e., $COV=\frac{\sigma}{\mu}\le\frac{\sqrt{(C_{\max}-\mu)(\mu-C_{\min})}}{\mu}$. Moreover, to avoid high densities (a U-shape is not suitable for geotechnical data) near the maximum bound (Fig. 4), it is necessary that $\beta \ge 1$, i.e.:

$$COV\le\left(\frac{C_{\max}}{\mu}-1\right)\sqrt{\frac{\mu-C_{\min}}{2C_{\max}-C_{\min}-\mu}} \quad (7)$$

With $\beta \ge 1$, this means that the cohesion values are correctly distributed (without high density near $C_{\max}$), for a COV ≤ 135%.

The generalized ARGUS distribution is less practical to use since its mean and standard deviation are expressed as functions that are too complex to be evaluated without mathematical software:

$$\mu_{ARGUS}=\int_0^{C_{\max}} x\ \mathrm{pdf}\,dx=C_{\max}\left[1-p\sqrt{\pi}\frac{\Gamma(p)}{\Gamma\left(p+\frac{5}{2}\right)}\left(\frac{\chi}{2}\right)^{2(p+1)}\frac{\mathrm{M}\left(p+1,p+\frac{5}{2},-\frac{\chi^2}{2}\right)}{\Gamma(p+1)-\Gamma\left(p+1,\frac{\chi^2}{2}\right)}\right] \quad (8)$$

with M being the confluent hypergeometric function of the 1st kind: $\mathrm{M}(a,b,x)=\sum_{n=0}^{\infty}\frac{(a)_n}{(c)_n}\frac{x^n}{n!}$ and where $(a)_n=\frac{(a+n-1)!}{(a-1)!}$ is the rising factorial.

$$\sigma_{ARGUS}=\sqrt{C_{\max}^2\left(\frac{\chi^2}{2}\right)^{p+1}\frac{e^{-\frac{\chi^2}{2}}+\left(\chi^2-2(p+1)\right)\left(\Gamma(2+p)-\Gamma\left(2+p,\frac{\chi^2}{2}\right)\right)}{(1+p)\left(\Gamma(1+p)-\Gamma\left(1+p,\frac{\chi^2}{2}\right)\right)}+C_{\max}\left(2\mu_{ARGUS}-C_{\max}\right)} \qquad (9)$$

Furthermore, the relations are not invertible and as a result, χ and p cannot be calculated analytically as a function of μ_{ARGUS} and σ_{ARGUS}. With a mean of 14.2 kPa, the maximum COV that can be achieved with ARGUS is 110% (σ= 15.62 kPa).

2.2 Continuous distributions defined on a semi-infinite interval

There are many distributions defined on a semi-infinite interval ([0; +∞[) that can reproduce the cohesion data with positive skewness (Table 2). Those tested all have at least 2 parameters, to simulate high COVs. Presuming the exclusion of the generation of invalid data above $C_{\max}$, excessively high cohesion values calculated using these distributions are subsequently right-censored; in cases where $C > C_{\max}$, C is constrained to $C_{\max}$. This process disturbs the calculation of μ and σ less than rejecting the data or truncating the distribution. The censored means and standard deviations are then calculated using the following formulae:

$$\tilde{\mu}=\int_{C_{\min}}^{C_{\max}} x\,\mathrm{pdf}(x)dx+C_{\max}\int_{C_{\max}}^{\infty}\mathrm{pdf}(x)dx \text{ and } \tilde{\sigma}=\sqrt{\int_{C_{\min}}^{C_{\max}} x^2\mathrm{pdf}(x)dx+C_{\max}^2\int_{C_{\max}}^{\infty}\mathrm{pdf}(x)dx-\tilde{\mu}^2} \qquad (10)$$

Table 2 shows the relative errors incurred when mapping densities from the interval [$C_{\max}$; ∞] to $C_{\max}$ for 6 distributions defined on a semi-infinite interval and for the normal distribution (for reference). The 6 semi-infinite distributions best able to reproduce both μ_C and σ_C are shown in Fig. 2.

Distribution/statistical parameter	Mean (kPa) $\mu=\tilde{\mu}(\mu_c,\sigma_c)\neq\mu_c$	Standard dev. $\sigma=\tilde{\sigma}(\mu_c,\sigma_c)\neq\sigma_c$	Relative error	COV
Data (unknown distribution)	μ_C = 14.2	σ_C = 20.3	-	143%
Normal (N)	17.1	16.2	28.8%	95 %
Log-normal (LN)	13.4	14.8	27.9%	110%
Inverse gaussian (IG)	13.4	15.7	23.2%	118%
Generalized inverse gaussian (θ=-0.33, GIG)	16.0	17.7	18.0%	111%
Generalized inverse-Gamma (γ=0.37, GIGA)	11.2	19.6	21.5%	175%
Birnbaum–Saunders (BS)	13.5	17.0	17.0%	126%
Generalized beta prime (θ=1.30, GBP)	17.3	14.4	36.3%	83%

Table 2 : Cohesion (kPa) distribution, means and standard deviations computed after censoring for different semi—infinite distributions, with initial statistical parameters for the cohesion (μ_C = 14.2 kPa, σ_C = 20.3 kPa).

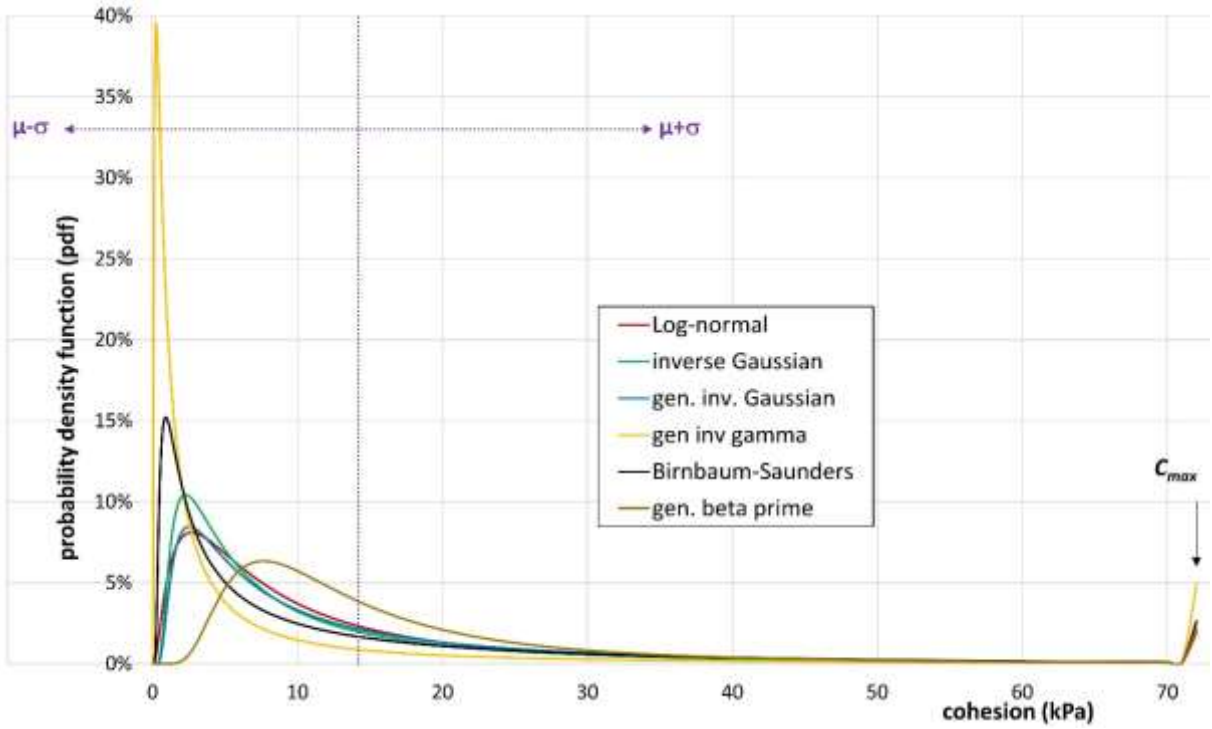

Fig. 2 : Distributions defined on a semi-infinite interval with initial parameters (μ_C, σ_C) for the cohesion, and after right-censoring.

To compensate for these errors, the parameters of these distributions have been modified so that the means and standard deviations calculated after right-censoring are equal to μ_c and σ_c. This amounts to numerically solving the system:

$$\begin{cases} \Delta\mu = \tilde{\mu} - \mu_C = 0 \\ \Delta\sigma = \tilde{\sigma} - \sigma_C = 0 \end{cases} \tag{11}$$

The analytical relations for the censored means and standard deviations ($\tilde{\mu}$ and $\tilde{\sigma}$) are complex and can be found in appendix B. The right-censored distributions are shown in Fig. 3. The effects of the censoring are visible near the minimum bound (C_{min} = 0 kPa): these semi-infinite distributions tend closely resemble the bounded interval distributions (Beta). All of these distributions are equivalent with respect to the objective of reproducing the data such that $\mu = \mu_C$ and $\sigma = \sigma_C$, but only the derived RAFF distribution has the desired behaviour at $x = C_{max}$. For the semi-infinite distributions, this undesired behaviour is due to the right-censoring (above C_{max}), but for the Beta distribution, this is due to the term $(C_{max} - x)^{\beta-1}$ that tends towards infinity when β<1 as x tends towards C_{max}. Table 3 shows the potentially large differences between the censored and non-censored parameters. The distance between these parameters shows which distributions are suitable for high COVs (low d).

Distribution	Mean	Standard deviation	Distance
	$\tilde{\mu}(\mu_r, \sigma_r) = \mu_C$	$\tilde{\sigma}(\mu_r, \sigma_r) = \sigma_C$	$d = \sqrt{(\mu_r - \mu_C)^2 + (\sigma_r - \sigma_C)^2}$
N	μ_r = -0.52	σ_r = 37.1	22.4
LN	μ_r = 23.6	σ_r = 107.7	87.9
IG	μ_r = 21.2	σ_r = 56.7	37.0

GIG (θ=-0.19)	μ_r = 8.7	σ_r = 22.7	6.0
GIGA (γ=0.37)	μ_r = 16.6	σ_r = 31.9	11.8
BS	μ_r = 16.3	σ_r = 28.9	8.8

Table 3 : Means, standard deviations and distances (kPa) computed after right-censoring for different distributions defined on semi-infinite intervals, with censored parameters

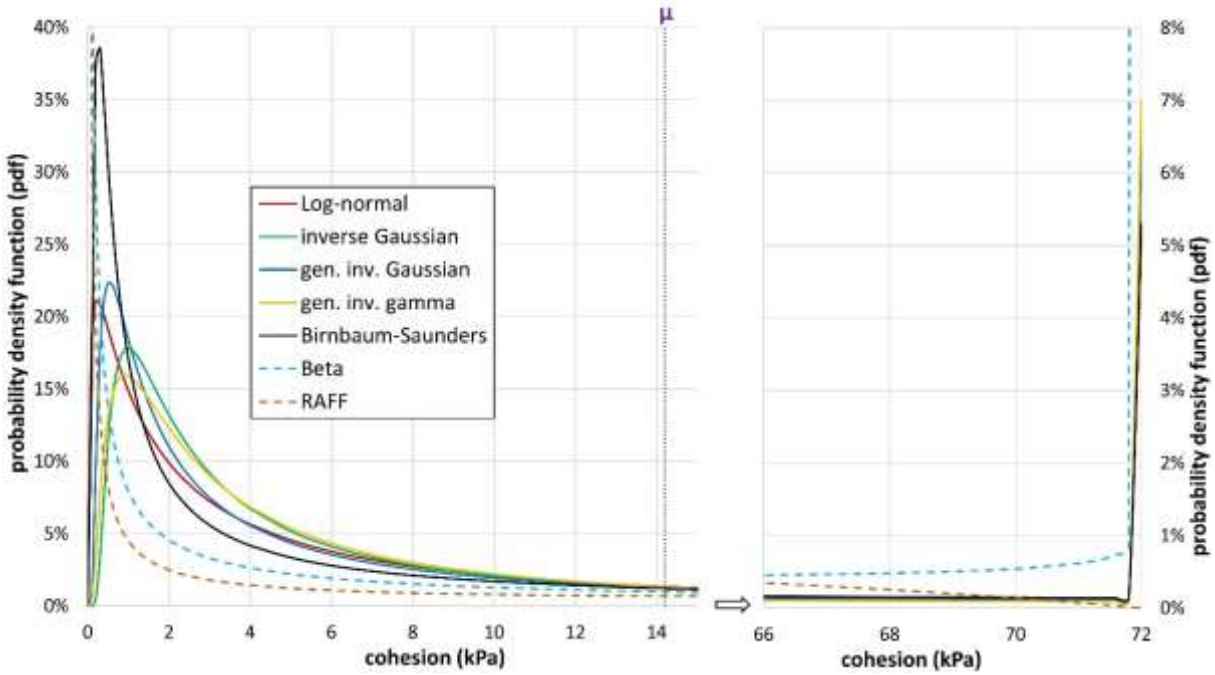

Fig. 3 : Best fit of 5 distributions of the cohesion defined on a semi-infinite interval (right-censored parameters are computed in order to have $\tilde{\mu}$ = μ_c = 14.2 KPa and $\tilde{\sigma}$ = σ_c = 20.3 kPa) compared to bounded distributions (Beta and RAFF).

2.3 New bounded interval distribution

The ARGUS and Beta distributions are not able to correctly reproduce the distribution of the measured cohesions. Considering the drawbacks inherent to each of these 2 distributions, we propose a new distribution based on the Beta distribution formula while drawing inspiration from the ARGUS distribution to prevent the increase of the Beta density in the vicinity of C_{max}. The formula of the distribution, called RAFF (Risk Assessment of Final pits during Flooding, a project supported by the Research Fund for Coal and Steel) in the rest of the paper, is the following:

RAFF: $$\text{pdf} = A\left(x-C_{\min}\right)^{\alpha-1}\left(C_{\max}-x\right)\text{e}^{-\beta\left(x-C_{\min}\right)} \quad (\alpha>0) \tag{12}$$

$$\text{CDF}=\frac{A}{\beta^{1+\alpha}}\left[\Gamma\left(1+\alpha,\beta\left(x-C_{\min}\right)\right)-\beta\left(C_{\max}-C_{\min}\right)\Gamma\left(\alpha,\beta\left(x-C_{\min}\right)\right)-\left(\alpha-\beta\left(C_{\max}-C_{\min}\right)\right)\Gamma\left(\alpha\right)\right] \tag{13}$$

with $$A=\frac{\beta^{1+\alpha}}{\Gamma\left(1+\alpha,\beta\left(C_{\max}-C_{\min}\right)\right)-\beta\left(C_{\max}-C_{\min}\right)\Gamma\left(\alpha,\beta\left(C_{\max}-C_{\min}\right)\right)-\left(\alpha-\beta\left(C_{\max}-C_{\min}\right)\right)\Gamma\left(\alpha\right)} \tag{14}$$

The term (C_{max} -x) was preferred to $\sqrt{C_{max}-x}$ or (C_{max}-x)² to avoid a distribution function lacking an analytical form, or to avoid one that is too complex, in the knowledge that the probability density functions would have similar profiles and that the parameters would be capable of reproducing a high COV. It should be noted that A (equation 14) is easily calculated for positive values of β. When β is

negative (the case for high COVs), the constant *A* remains a real number even if its individual elements are complex numbers. It can be shown that if $\beta < 0$, then $\beta = |\beta|^{1+\alpha} e^{i\pi(1+\alpha)}$, $\Gamma(\alpha,\beta) = \Gamma(\alpha) + e^{i\pi(1+\alpha)} \int_0^{-\beta} x^{\alpha-1} e^x dx$.

After simplifications, we verify that *A* is a ratio of positive real numbers:

$$A(\beta<0) = \frac{|\beta|^{1+\alpha}}{\beta(C_{\min}-C_{\max}) \int_0^{\beta(C_{\min}-C_{\max})} x^{\alpha-1} e^x dx - \int_0^{\beta(C_{\min}-C_{\max})} x^{\alpha} e^x dx} > 0 \quad (15)$$

This explains that $\int_0^{\infty} (x-C_{\min})^{\alpha-1} (C_{\max}-x) e^{-\beta(x-C_{\min})} dx = \frac{1}{A}$ regardless of the sign of β.

For a negative β, it is best to evaluate *A* with Mathematica-type mathematical software (or to program relation 15), since the algorithms able to compute the incomplete Gamma function with a negative value of β are complex and remain a topic of research in applied mathematics [41]. For $\beta > 0$, $\Gamma(\alpha, \beta)$ can be calculated with Excel (using the Gamma function and the Gamma distribution: $\Gamma(\alpha,\beta) = \Gamma(\alpha)$ (1-CDF $\Gamma(\alpha, \beta)$). For $\beta = 0$, the distribution remains defined and becomes:

$$\lim_{\beta\to 0} \text{pdf} = \frac{\alpha(1+\alpha)}{(C_{\max}-C_{\min})^{1+\alpha}} (x-C_{\min})^{\alpha-1} (C_{\max}-x) \quad \mu_{RAFF}^{\beta\to 0} = \frac{2C_{\min}+\alpha C_{\max}}{2+\alpha} \quad \sigma_{RAFF}^{\beta\to 0} = \frac{C_{\max}-C_{\min}}{2+\alpha}\sqrt{\frac{2\alpha}{3+\alpha}} \quad (16)$$

To streamline the subsequent equations, we will assume that $C_{\min} = 0$, aligning with the actual conditions of the cohesion measurements. The mean and standard deviation have formulae with a level of complexity intermediate between that of Beta and ARGUS:

$$\mu_{RAFF} = \frac{\beta C_{\max}(\Gamma(1+\alpha) - \Gamma(1+\alpha,\beta C_{\max})) + \Gamma(2+\alpha,\beta C_{\max}) - \Gamma(2+\alpha)}{\beta((\beta C_{\max}-\alpha)\Gamma(\alpha) - \beta C_{\max}\Gamma(\alpha,\beta C_{\max}) + \Gamma(1+\alpha,\beta C_{\max}))} \quad (17)$$

$$\sigma_{RAFF} = \sqrt{\frac{\beta C_{\max}(\Gamma(2+\alpha) - \Gamma(2+\alpha,\beta C_{\max})) + \Gamma(3+\alpha,\beta C_{\max}) - \Gamma(3+\alpha)}{\beta^2((\beta C_{\max}-\alpha)\Gamma(\alpha) - \beta C_{\max}\Gamma(\alpha,\beta C_{\max}) + \Gamma(1+\alpha,\beta C_{\max}))} - \mu_{RAFF}^2} \quad (18)$$

The fact that these 2 statistical parameters depend on the Gamma function (incomplete or not) does not make it possible to analytically link the 2 shape parameters α and β to μ and σ. With a mean of 14.2 kPa, a COV of 200% (σ = 28.4 kPa) can be achieved with the RAFF distribution. Fig. 4 represents the probability densities function (pdf) for different COV values. For the cohesion data of a mining deposit (COV = 143%), the distribution obtained with RAFF fulfils the objectives set: reproduction of μ = 14.2 kPa and σ = 20.3 kPa without censoring, and with a positive skewness. To reproduce high COVs (110%<COV<200%), the α and β parameters vary over restricted intervals: $-2 < \beta < 0$ and $10^{-59} < \alpha < 0.5$ (Fig. 5). Contrary to what the "COV RAFF = 200%" curve (Fig. 4) may suggest, the higher the COV, the greater the weight of the distribution near $C_{\min}$ becomes.

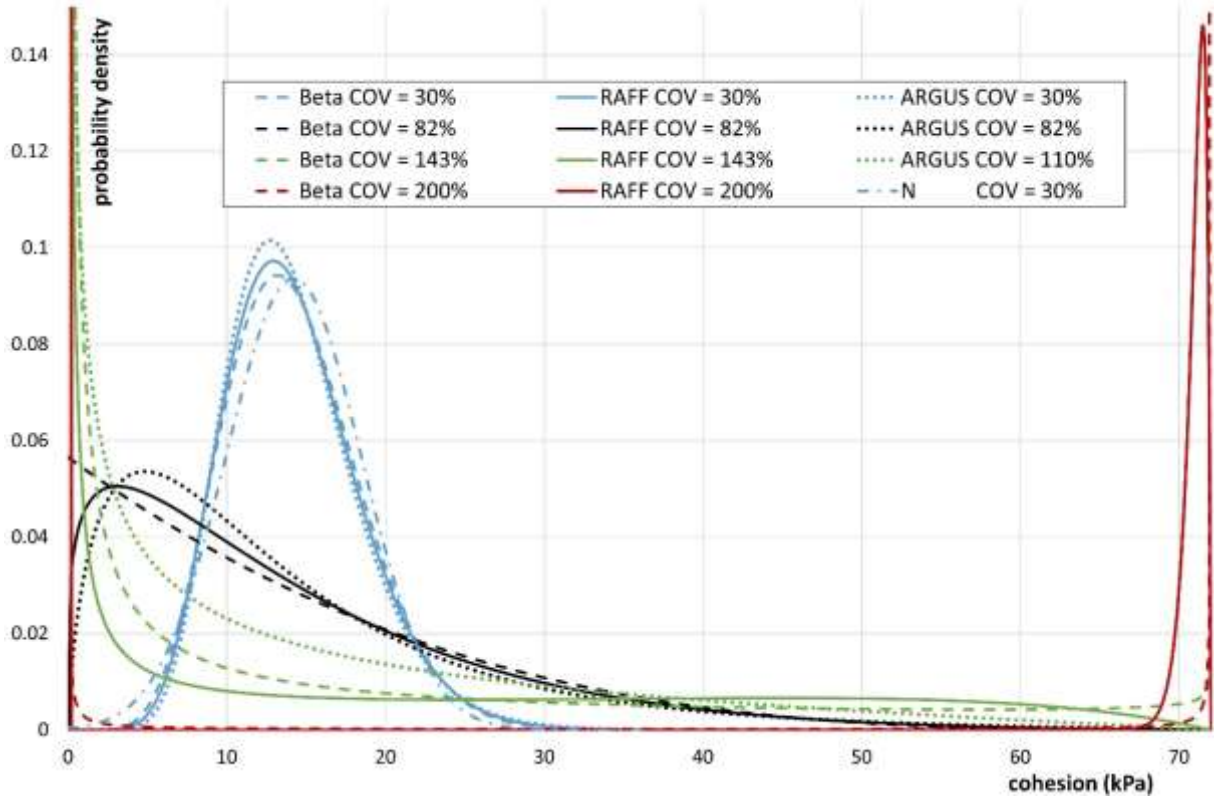

Fig. 4 : Comparison of 4 distributions defined on a bounded interval, for different COV values

For a COV of 200%, 80% of the data falls between C_{min} and C_{min} +10% (C_{max} -C_{min}), while the remaining 20% is distributed between C_{max} -10% (C_{max} -C_{min}) and C_{max} (Fig. 5). Given this high level of dispersion, the data naturally clusters around the two extreme values (C_{min} and C_{max}).

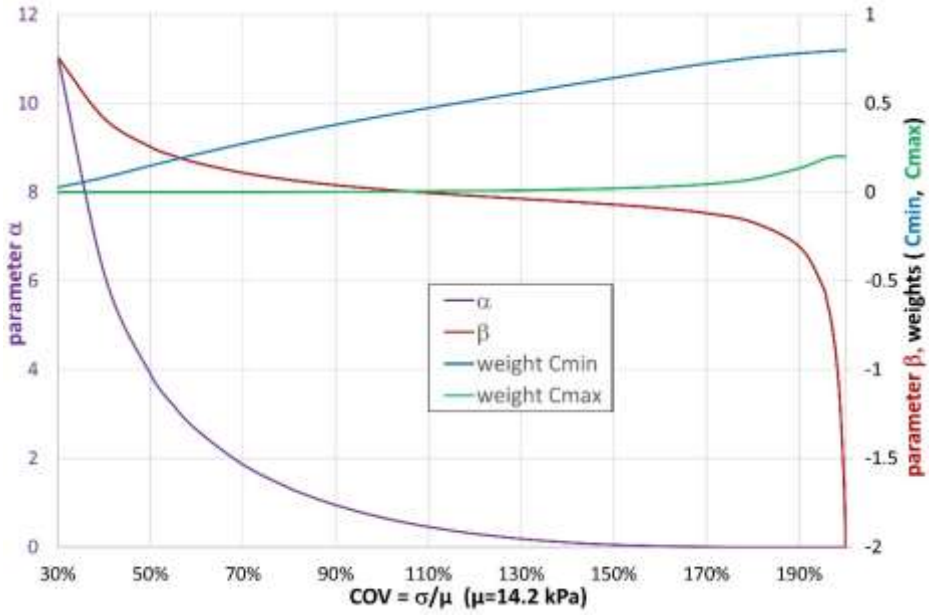

Fig. 5 : Evolution of parameters α and β (RAFF distribution) and of weights near C_{min} and C_{max} as a function of the coefficient of variation (COV)

Apart from the constant A (which can be calculated in advance for given α and β), the RAFF probability density function (pdf) does not make use of special functions which are difficult to evaluate in software. Unfortunately, this is not the case for the RAFF cumulative distribution function (necessary for the

RAFF random number generator) which contains the term $\Gamma\left(\alpha,\beta\left(x-C_{\min}\right)\right)$. This drawback can be circumvented by using its series expansion in the vicinity of 0:

$$\mathrm{CDF}(x=C_{\min}=0)=\frac{\beta^{1+\alpha}x^{\alpha}\left[\sum_{i=1}^{n}B_i x^i-\frac{C_{\max}}{\alpha}+O\left(x^{n+1}\right)\right]}{\left(\alpha-\beta C_{\max}\right)\Gamma\left(\alpha\right)+\beta C_{\max}\Gamma\left(\alpha,\beta C_{\max}\right)-\Gamma\left(1+\alpha,\beta C_{\max}\right)} \tag{19}$$

with $B_i=\left(i+\beta C_{\max}\right)\frac{\left(-1\right)^{i+1}\beta^{i-1}}{\left(i+\alpha\right)i!}$

Because this is an expansion in the vicinity of 0, the maximum error occurs at $x = C_{max}$. This can be effectively improved by changing the coefficient of x^n so that CDF = 1 at $x = C_{max}$. The relation (19) then becomes:

$$\mathrm{CDF}=\frac{\beta^{1+\alpha}x^{\alpha}\left[\sum_{i=1}^{n}B_i x^i-\frac{C_{\max}}{\alpha}-\frac{x^n}{C_{\max}^n}\left(\sum_{i=1}^{n-1}B_i C_{\max}^i-\frac{C_{\max}}{\alpha}\right)+O\left(x^{n+1}\right)\right]}{\left(\alpha-\beta C_{\max}\right)\Gamma\left(\alpha\right)+\beta C_{\max}\Gamma\left(\alpha,\beta C_{\max}\right)-\Gamma\left(1+\alpha,\beta C_{\max}\right)}+\frac{x^{n+\alpha}}{C_{\max}^{n+\alpha}} \tag{20}$$

With a polynomial of order 14, the maximum relative and absolute errors can be limited to the machine precision (10^{-16}), whereas these can increase to 2.10^{-5} when using relation (19). Fig. 6 illustrates the improvement achieved in comparison to relation (19): for $n \geq 5$, the error is less than 10^{-n} when using (20). The distribution and probability density functions of the RAFF distribution using the parameters that enable the reproduction of the cohesion data of [35] are shown in Fig. 7.

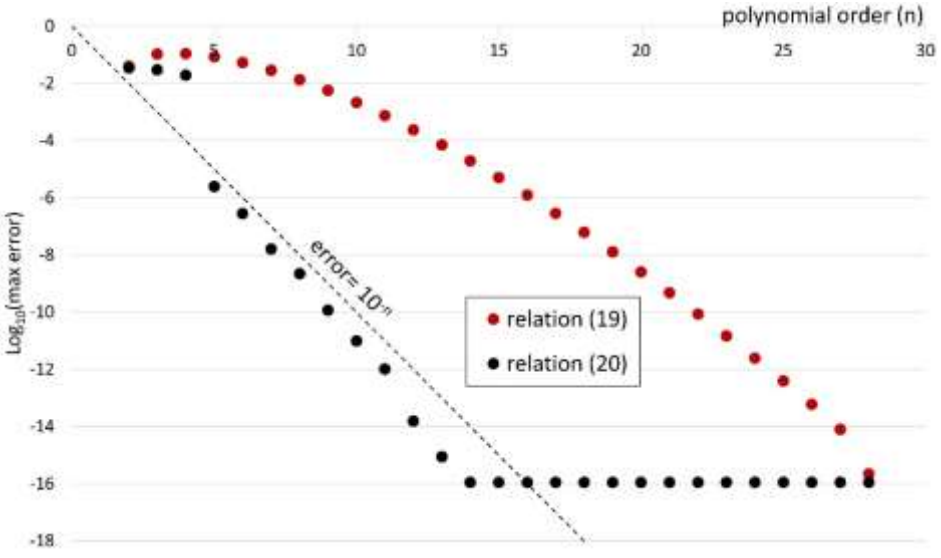

Fig. 6 : Comparison of maximum errors for series expansions (original and modified) of the RAFF CDF

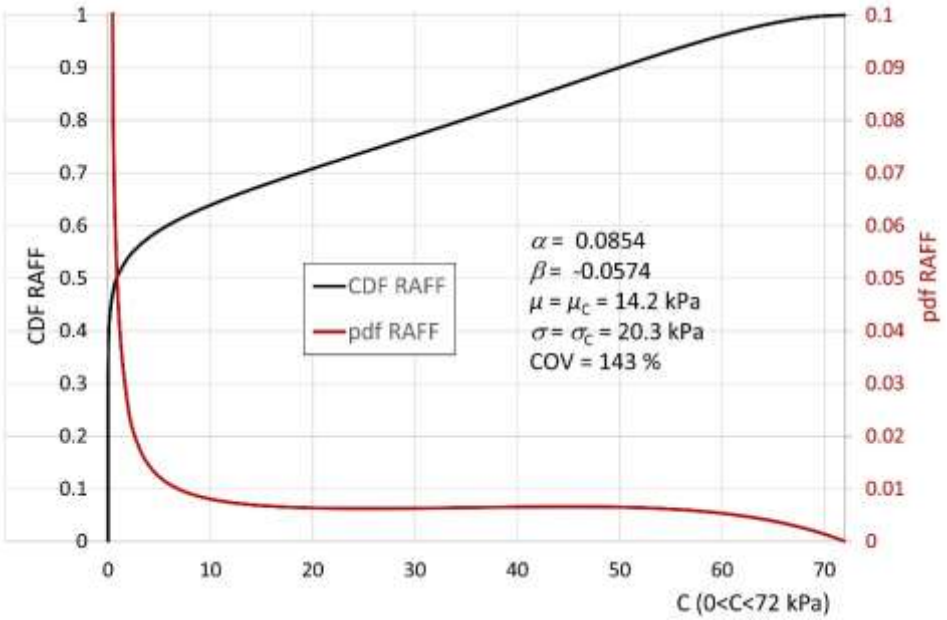

Fig. 7 : Cumulative (CDF) and probability density functions (pdf) of the RAFF distribution that reproduces the cohesion data of [35].

It is not possible to determine the RAFF quantile function ($w(p)=C$ if p=CDF(C)) using the Lagrange-Bürmann inversion theorem because the RAFF CDF is not an analytic function (equations (19) and (20) are not formal series because of the non-integer power of x^{α}).

However, it is possible to approximate the quantile function by postulating the following relations:

- if 0<p<CDF(C_1): $w(p)=p^{a}\sum_{i=1}^{15}D_i p^{i}$ (a close to $1/\alpha$), with C_1 = 50 kPa
- if CDF(C_1)<p<CDF(C_2): $w(p)=E_1+E_2\tan\frac{E_3+E_4 p+E_5 p^2+E_6 p^3}{E_7+E_8 p+E_9 p^2+E_{10} p^3+E_{11} p^4}$, with C_2 = 69 kPa
- if CDF(C_2)<p<1: $w(p)=F_1+F_2\tan\frac{F_3+F_4 p+F_5 p^2+F_6 p^3}{F_7+F_8 p+F_9 p^2+F_{10} p^3+F_{11} p^4}$

With these relations, the maximum absolute error is less than 0.0125 kPa. For the random values of the cohesion Ci greater than 1 kPa, the maximum relative error is 0.025%. For mining, civil engineering or geomechanical applications, this cohesion error is acceptable and simplifies the generation of random variables for the RAFF distribution.

2.4 Comparison of different distributions

To compare the ability of the different continuous distributions of positive variables (distributions with semi-infinite intervals being censored) to represent specific mean and standard deviation pairs, we determined the envelope curves in (μ,σ) space, as illustrated in Fig. 8 (where the variable X is the cohesion). The envelope curves correspond to the extreme case where one part of the data is equal to the minimum value ($X_i = X_{min}$, i from 1 to m) and the other part is equal to the maximum value (X_i = X_{max}, i from m+1 to n). The expectations for X and X^2 are therefore: $\mathrm{E}[X]=X_{max}-\frac{m}{n}(X_{max}-X_{min})$ and $\mathrm{E}[X^2]=X_{max}^2-\frac{m}{n}(X_{max}^2-X_{min}^2)$.

The expectation for X^2 can also be written: $\mathrm{E}\left[X^2\right]=\mathrm{E}[X]\left(X_{\max}+X_{\min}\right)-X_{\max}X_{\min}$. Taking equation (10), we thus obtain:

$\sigma\le\sqrt{\mu\left(X_{\max}+X_{\min}\right)-X_{\max}X_{\min}-\mu^2}$ or in standard form: $\frac{2\sigma}{X_{\max}}\le\sqrt{F-\left(\frac{2\mu}{X_{\max}}-G\right)^2}$

with $F=\left(\sqrt{2}+1-\frac{X_{\min}}{X_{\max}}\right)\left(\sqrt{2}-1+\frac{X_{\min}}{X_{\max}}\right)$ and $G=1+\frac{X_{\min}}{X_{\max}}$ (these 2 constants are ≥1 for the positive random variables). Here we can see the equation of a circle with centre ($\mu=\frac{X_{\min}+X_{\max}}{2}$; 0) and radius $\sqrt{F}$. For the case where $X_{\min}$ =0, this is simplified with F=G=1 and $\frac{2\sigma}{X_{\max}}=\sqrt{1-\left(\frac{2\mu}{X_{\max}}-1\right)^2}$.

Note that the GIG (Generalised Inverse Gaussian) distribution is not shown in Fig. 8 because its range of validity has been maximised by its 3rd parameter, which does not make it comparable with other (2-parameter) distributions. The RAFF and Beta distributions with β<1 (U-shape) have a validity range equivalent to this theoretical limit. In Figure 8, we present the (μ, σ) data for both cohesion C and friction angle ϕ, incorporating the typical variation intervals observed for C and ϕ. In contrast to cohesion C, where coefficients of variation (COVs) are generally of substantial magnitude, the COVs associated with friction angle ϕ are moderate. This suggests that a normal distribution N can be employed to assess the variability of ϕ.

In general, the closer these envelopes are to the theoretical limit, the better the distribution in question can correctly reproduce the pair (μ_C, σ_C). However, given the sometimes-complex evolution of these limits, it is best to choose the distributions whose envelopes are closest to (μ_C, σ_C). In our case, the most interesting semi-infinite and bounded interval distributions are respectively the BS and RAFF distributions.

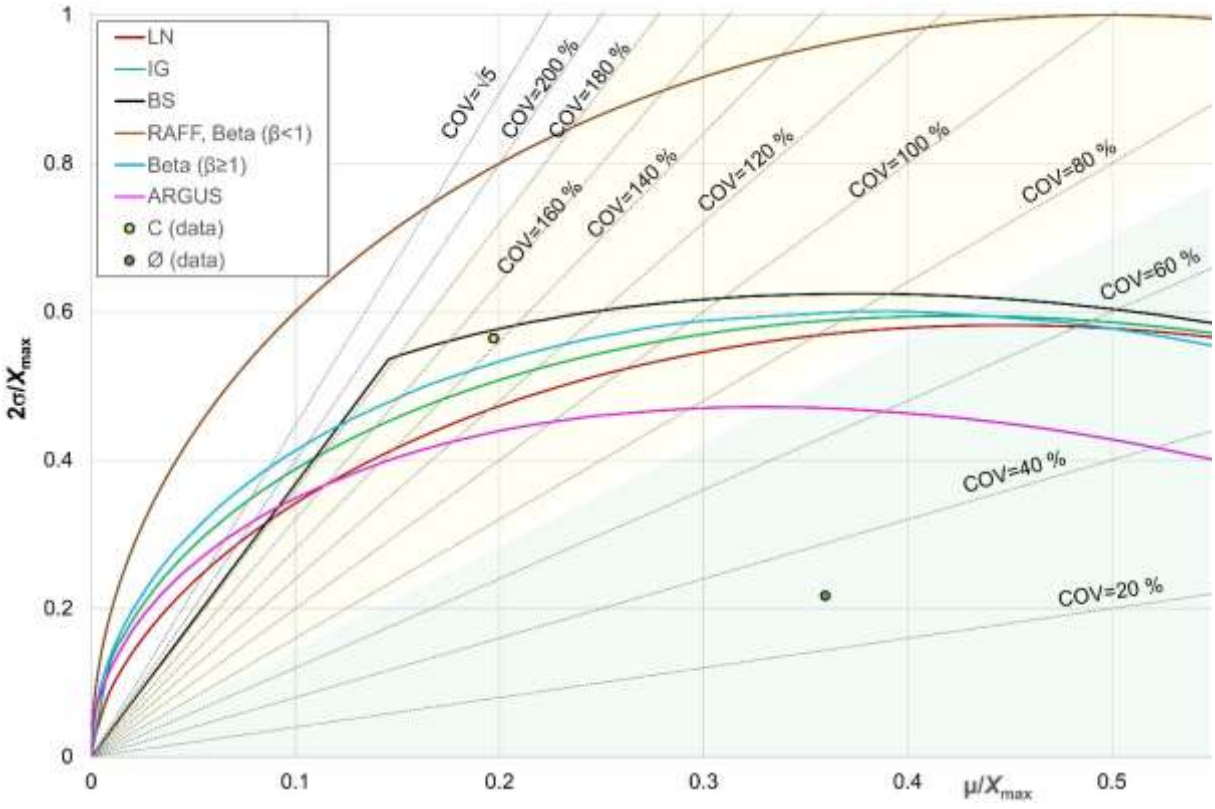

Fig. 8 : Range of validity (μ/C_{max}, $2\sigma/C_{max}$) of different continuous distributions (unbounded distributions having been censored), range of variation of the COV for cohesion (yellow) and friction angle (green).

The BS distribution (for which COV<$\sqrt{5}$) has a noticeable restricted domain of validity in comparison to that of the other distributions. The Beta ($\beta < 1$) and RAFF distributions have larger domains of validity (>40%) than the other distributions, but if the U-shape is to be avoided, the Beta $\beta < 1$) distribution ends up being no more preferable than the semi-infinite distributions. On the other hand, the domain of validity of the ARGUS distribution is restricted by the values of the standard deviation; it is not possible to simulate data with a standard deviation higher than 0.236 C_{max}. In conclusion, this figure underscores the challenge of identifying a distribution that accurately replicates data with a high coefficient of variation (COV) when both the standard deviation and mean are elevated. For instance, the dataset (μ = 0.33 C_{max}, σ = 0.472 C_{max}) exhibits a COV of 143%. But except for RAFF, none of the distributions - excluding Beta with β < 1 due to infinite density at C_{max} - can effectively capture this specific dataset.

These first results show the superiority of the proposed probability distribution in reproducing the behaviour of materials with a very high spatial variability.

3 Data generation with RAFF distribution

3.1 Random variable generators

After having developed and identified the distributions capable of reproducing the distribution of the cohesion (RAFF) and of the friction angle (N), the objective is to generate populations of data corresponding to these distributions. This is the role of the random variable generator, which is based on the search for the random variable $X = F^{-1}(u)$ with $u \int Y_{(0,1)}$, F being the cumulative distribution function (CDF). Knowing that F is not always defined (case of GIG), or, conversely, given that F^{-1} is known, three methods exist to build a random generator.

The first and simplest method is the one for which the analytical solution of the inverse of the distribution function is known. The analytical forms of F^{-1} for the N, LN and BS distributions (table in the appendix) depend on the inverse of the error function (Erf^{-1}). This function has usually been implemented in software, which solves the problem.

The 2nd method consists of a specific (existing) algorithm. The most famous is probably the Box-Muller transformation [42] which makes it possible to generate a normal random variable using:

$$X = \sqrt{-2\ln(u_1)}\cos(2\pi u_2)\sigma + \mu \tag{21}$$

with u_1 and u_2, being two uniform random variables.

It is also possible to use the effective approximations of Erf^{-1}, such as that developed by [43]:

$$\mathrm{Erf}^{-1}(x) \approx \mathrm{sgn}\,x \sqrt{\sqrt{B^2 - \frac{\ln(1-x^2)}{a}} - B} \text{ with } a = \frac{8(\pi-3)}{3\pi(4-\pi)} \text{ and } B = \frac{2}{\pi a} + \frac{\ln(1-x^2)}{2} \tag{22}$$

The algorithm may include a more or less complex test. For example, for the inverse Gaussian distribution [44]:

1) Generation of $Y = \mathrm{N}^{2}_{(0,1)}$ and $X = \mu + \frac{\sigma^2}{2\mu}\left(Y - \sqrt{Y^2 + 4\frac{\mu^2}{\sigma^2}Y}\right)$ (23)

2) Test: if $X > \left(\frac{\mu}{\mathrm{U}_{(0,1)}} - \mu\right) \Rightarrow X = \frac{\mu^2}{X}$

The 3rd method consists in creating one's own algorithm if it does not exist or if its domain of validity is incompatible with the needs of the study. For example, this is the case of the GIG distribution for which generators exist [45,46,47,48], but in addition to their complexity, they do not guarantee the validity of the results for all combinations of their 3 parameters. It is then necessary to solve F(*X*)=*u* numerically. There are then 2 specific cases depending on whether F is defined or not defined. If F is defined, Newton's method is very effective with a suitable initial value. Thus, it is sufficient to iterate *n* times the relation: $x_0 = x_0 - \frac{\mathrm{F}(x_0) - u}{\mathrm{f}(x_0)}$ with $u \int \mathrm{Y}_{(0,1)}$ and x_0 = distribution mode. In practice, *n* = 11 is sufficiently precise to generate values for the cohesion random variable. However, even when defined, F may be too complex (relation 13) to be programmed as it stands. In this case, it is effective to use a series expansion of F, which is simply a polynomial calculation (relation 19). If F is not defined, F(x_0) is at any rate an integral form which must then be evaluated numerically.

3.2 Cohesion and friction angle correlation

The cohesion and the friction angle are generally correlated, a known correlation for soils [49]. The random generation of the Mohr-Coulomb failure criterion parameters must consider the correlation between the two parameters ϕ and *C*. It is known that simplified probabilistic analysis, in which spatial variability is ignored by assuming perfect correlation, can lead to an underestimated probability of failure [3]. The values of the correlation *r* vary between -0.11 and -0.83 [50]. For the remainder of this study, the value of *r* = -0.5 was adopted (even if for a real case, *r* can vary according to the clay content). The consequence of this choice is that the distribution of the friction angle is no longer an identified distribution (like the normal distribution, Fig. 1), but a distribution capable of reproducing *r* = -0.5, μ_ϕ and σ_ϕ while varying between ϕ_{min} and ϕ_{max}.

From a practical point of view, it is preferable to be able to generate the friction angles at the same time as the cohesions without having to restart the generation of these 2 variables if the correlation coefficient is too far from the desired value (with *r* = -0.5). The common method to establish a correlation (with a correlation coefficient *r*) between the variable *Y* and the variable *X* from any distribution Δ involves setting [51]:

$$Y = \left(\frac{\mathrm{D} - \mu_X}{\sigma_X} r + N\ (0,1)\sqrt{1-r^2} \right) \sigma_Y + \mu_Y \qquad (24)$$

The major drawback of this procedure is that it generates *Y* values without considering the possible range of variation of *Y*. With the data from this study, up to 8% of the friction angles are greater than 38° or less than 8°. To limit this problem, other distributions than $\mathrm{N}(0,1)$ were tested. Since ϕ *(Y)* is distributed in the interval [ϕ_{min}; ϕ_{max}], the candidates (Beta, Wigner semicircle and Marchenko-Pastur, Table 4) are bounded interval distributions whose PDF profiles are compatible with that of N. Note that ϕ (negative skewness) cannot be distributed with RAFF, which is defined for positive skewness. The random variable ϕ (correlated to *C* via *r*) is generated by the following relation assuming an initial distribution Δ_ϕ: $\phi = \left(\frac{\mathrm{D}_C - \mu_C}{\sigma_C} r + \frac{\mathrm{D}_\phi - \mu_\phi}{\sigma_\phi} \sqrt{1-r^2} \right) \sigma_\phi + \mu_\phi$ (25)

To assess the effectiveness of Δ_ϕ, 5 x 4 x 20,000 draws from a population of 793 individuals (corresponding to the number of grid cells in the slope discussed in the following chapters) were carried out with the 5 cohesion distributions (N, LN, GIG, BS and RAFF) coupled to the 4 Δ_ϕ distributions. The analysis of the results showed that the Δ_ϕ = Beta distribution is more effective than the others. As regards the Wigner distribution, this is not surprising since it itself can be reduced to a specific Beta distribution (with α=β=3/2). Table 4 is an example of these results with Δ_C = RAFF. Depending on the distribution of *C*, the rejection rate varies between 2.70% (GIG) and 3.20% (N). The

error on the mean of ϕ with Δ_ϕ = Beta varies between 0.10% (RAFF) and 0.18% (BS). The error on the standard deviation of ϕ with Δ_ϕ = Beta varies between -1.22% (RAFF) and -1.86% (LN). RAFF is the distribution of *C* that best generates the correlated values of the variable ϕ. Using Δ_ϕ = Beta instead of $\mathrm{N}(0,1)$ reduces the rejection rate by 43%, the error on the mean by 64% and the error on the standard deviation by 73%. The random values of Δ_ϕ = Beta are generated with Johnk's algorithm:

$$\mathrm{D}_\phi = \frac{\mathrm{U}_{1(0,1)}^{\frac{1}{\alpha_\phi}}}{\mathrm{U}_{1(0,1)}^{\frac{1}{\alpha_\phi}} + \mathrm{U}_{2(0,1)}^{\frac{1}{\beta_\phi}}} \text{ if } \mathrm{U}_{1(0,1)}^{\frac{1}{\alpha_\phi}} + \mathrm{U}_{2(0,1)}^{\frac{1}{\beta_\phi}} \leq 1 \tag{26}$$

Parameters α_ϕ and β_ϕ are calculated using relations (5) and (6).

Distribution	$\phi_{\min}$; $\phi_{\max}$	Rejection rate (mean [min ; max])	μ/μ_ϕ-1	σ/σ_ϕ-1
Beta	-0.61 ; 40.0	3.18% [0.63% ; 5.68%]	0.10%	-1.22%
Wigner semicircle	1.33 ; 42.1	4.95% [2.27% ; 8.32%]	-0.07%	-1.87%
Normal	-18.1 ; 64.6	5.54% [2.40% ; 8.95%]	-0.28%	-4.58%
Marchenko-Pastur	3.35 ; 44.2	6.27% [2.90% ; 9.84%]	-0.33%	-2.94%

Table 4 : Rejection rates for various assumed distributions of ϕ, based on the results of 20,000 draws involving 793 items, with *C* distributed according to RAFF.

Since the Beta distribution is defined on the interval [0, 1], the relation to generate a random variable ϕ correlated to *C* with a correlation coefficient *r* is the following:

$$\phi = \left(\frac{\mathrm{D}_C - \mu_C}{\sigma_C} r + \frac{(\phi_{\max} - \phi_{\min})\mathrm{Beta}(\alpha_\phi, \beta_\phi) + \phi_{\min} - \mu_\phi}{\sigma_\phi} \sqrt{1 - r^2} \right) \sigma_\phi + \mu_\phi \tag{27}$$

4 Discussion and conclusion

4.1 Application test for slope stability analysis

The numerical approach of strength reduction method (involving friction angle and cohesion, and also known as "*C*-ϕ reduction") is used to numerically calculate slope stability [49,50,51]. The mean principle of the method is to reduce the initial values of the friction angle and the cohesion until a factor of safety equal to 1 (FoS=1) is obtained. The numerical model that will serve as an example for probabilistic calculations is shown in Fig. 9. It corresponds to the mining deposit slope around Lake Most [50] with a slope angle of 24°. The assumption of a spatially distributed pattern of geomechanical properties is warranted, particularly in the case of mine deposits comprised of reworked waste rock, tailings, and other highly heterogeneous materials. To perform the stability calculation, the software adopted (Flac3D, [52]) uses the strength reduction method. The surface of the model is discretised into meshes. Each mesh can be assigned specific values for geomechanical properties, allowing for the spatial distribution of cohesion and friction angle in accordance with a particular distribution (see Fig. 10) featuring a specific spatial correlation. It is essential to ensure an adequate number of meshes to mitigate any substantial bias, comparable to the approach employed in [3].

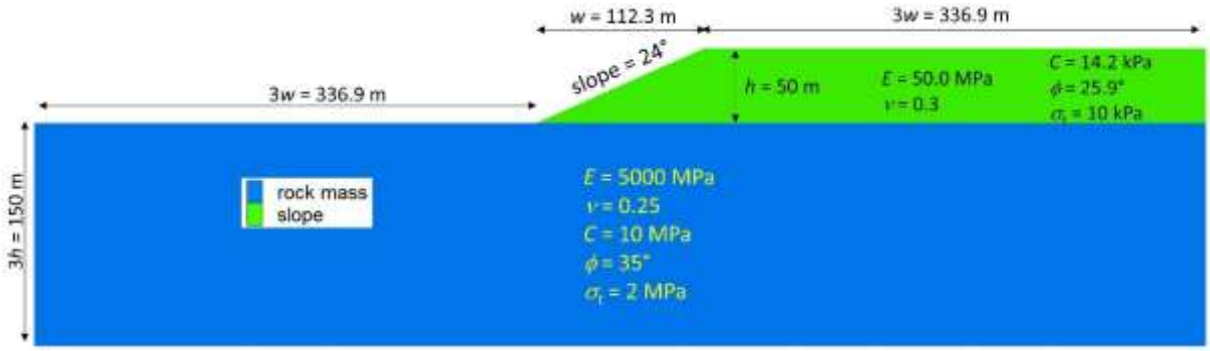

Fig. 9 : Geometry and average properties of the numerical model for the study of slope stability of a deposit (Most lake example, **Erreur ! Source du renvoi introuvable.**).

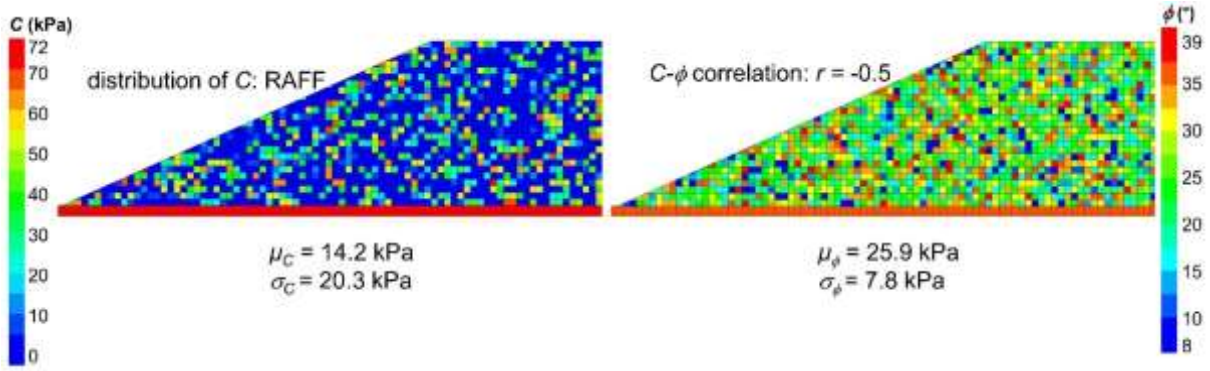

Fig. 10 : Distributions of cohesion C and friction angle ϕ in the deposit upper layer (Fig. 9): data taken from Masoudian et al. (2019).

To show the contribution of the new distribution to the stability analysis of a slope, 3 calculations were carried out: 2 Monte-Carlo simulations with RAFF and LN distributions, and a deterministic calculation using uniform properties. For this purpose, 256 random draws of (C_i, ϕ_i, r=-0.5) were made with the RAFF and Log-normal distributions, while reproducing μ_C, σ_C, μ_ϕ and σ_ϕ. The results of these calculations (Fig. 11) show the influence of the distribution of C on the distribution of FoS. All these distributions can be compared to the deterministic calculation (FoS = 1.47) where all the meshes of the slope have the cohesion μ_C and the friction angle μ_ϕ. The high mean of the LN distribution is due to the strong influence of right-censoring above C_{max}: it is an assumed bias that contributes to artificially increasing the weight of the distribution near the maximum bound. Conversely, this bias does not exist with a bounded interval distribution (RAFF), which explains why the mean FoS with an LN distribution for C is up to 19% higher than the mean FoS computed using a RAFF distribution. Similarly, the standard deviation of the FoS with RAFF distribution for C is 90% higher than using an LN distribution for C. The choice of the C distribution is therefore of paramount importance in view of its significant impact. With a steeper geometry, resulting in FoS values shifted by -0.2, a noteworthy portion of the RAFF probability densities (excluding LN) would then fall below 1. This would lead to significantly distinct rupture probabilities for the RAFF distribution. These results show that unbounded distributions (such as LN) tend to increase μ_{FoS} and decrease σ_{FoS}, which underestimates the probability of failure compared to the RAFF bounded distribution.

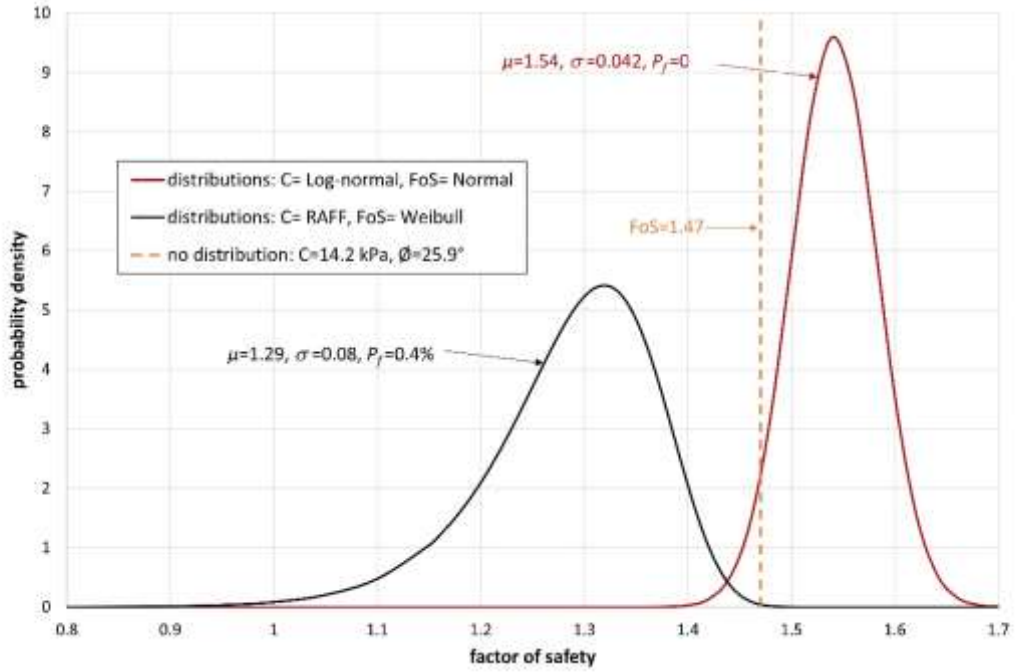

Fig. 11 : Influence of *C* distributions on the FoS distribution (normal or Weibull), *r* = -0.5.

4.2 Discussion

The discussion concerns the role of the choice of the right representative distribution of the cohesion for highly heterogeneous soils. The Log-normal distribution is a popular choice in the geotechnical engineering field for the cohesion of soil (being a strictly non-negative property). And if this distribution can reproduce data with a high COV, this is only possible under certain conditions for μ_C and σ_C. For example, a COV of 143% is reached with LN if $\mu_C < 0.143\ C_{max}$ (in this case: $\sigma_C < 0.203\ C_{max}$, Fig. 8): these limit values are 28% lower than the data used in this article ($\mu_C = 0.197\ C_{max}$ and $\sigma_C = 0.282\ C_{max}$). In general, semi-infinite distributions can reproduce high COVs but only with limited standard deviations (often less than $0.3\ C_{max}$). In addition, the errors made with censorship on the right are very important with high COVs (since the right tail has a greater weight in the distribution). With equation (10), μ_C = 14.2 kPa, σ_C = 20.3 kPa (COV=143%) and C_{max} = 72 kPa, errors on the means and standard deviations are $\Delta\mu$ = -6 % and $\Delta\sigma$ = -27 %. With a lower COV (50 %), i.e., μ_C = 14.2 kPa, σ_C = 7.1 kPa, errors on μ and σ become negligible: $\Delta\mu$ = -0.008% and $\Delta\sigma$ = -0.1%. To avoid questions about data censoring, the best solution is to adopt a bounded interval distribution such as RAFF, which is capable of reproducing data with a high COV.

In fact, given the importance of the right-censoring of semi-infinite distributions, it is important to ask whether the right-censoring accurately represents the distribution of data near the maximum cohesion value C_{max}. If the measurement interval is bounded, this means that at least one measurement is equal to C_{max}. As the mean and standard deviation were calculated with 27 measurements, this means that the probability of the last bin of *C* is at least 3.7%, which is close to $\int_{C_{max}}^{\infty} \mathrm{pdf}(x)dx$ for the semi-infinite distributions studied in this paper. The argument that right-censoring accurately represents that data distribution near C_{max} can be dismissed for two reasons. The first is that it is enough to add an *n*+1st bin (if the data is divided into *n* bins with width ΔC) which would be assigned zero frequency. But with censoring, it is this bin that would be assigned a probability equal to $\int_{C_{max}+\Delta C}^{\infty} \mathrm{pdf}(x)dx$ instead of 0. The second reason relates to the rejection of exceptional values. Indeed, a value higher than Q3+1.5(Q3-Q1) can be considered as exceptional and can therefore be rejected (Q1 and Q3 are the 1st and 3rd quartiles). Conversely, a cohesion cannot be less than Q1-1.5(Q3-Q1) because this quantity is negative

when the data are mostly concentrated near the minimum bound (0): no low value can therefore be rejected. The tests carried out with the different (cohesion) distributions of this study all showed that C_{max} > Q3+1.5(Q3-Q1) which reinforces the idea that the distribution must be strictly decreasing in the vicinity of C_{max} and that consequently, a bounded interval distribution (which respects this decrease) is preferable to a semi-infinite distribution (which does not respect this decrease because of the right-censoring).

4.3 Conclusion

The probabilistic calculation of the slope stability of highly heterogeneous soils such as mine deposits requires an adapted distribution. The terrains of the mine deposits correspond to a material with a very high coefficient of variation of the cohesion (143% for the example discussed here). This high level of dispersion made it necessary to develop a new bounded interval distribution (RAFF) capable of reproducing such a high variability (up to COV=200%). Relations (sometimes approximate) were developed to build the random generator for this new distribution. Given the frequent exploration of the correlation between cohesion and friction angle, a specialized relationship was formulated to generate friction angles with a targeted correlation coefficient. This approach prioritizes adherence to the designated range of phi by minimizing rejections or by interval-censoring. The results obtained with the new distribution are compared to four other semi-infinite distributions that have been censored to respect the variation domains of the randomly distributed parameters. A figure illustrating the domains of validity for various distributions (Fig. 8) has been specifically constructed to determine whether the data corresponds to an extreme case, necessitating adoption of the RAFF distribution.
The newly introduced bounded distribution (RAFF) underwent testing using cohesion data sourced from mining deposits within the framework of slope stability calculations (MCS) reproducing the geometry of the banks of Lake Most (Czech Republic).

The choice of the distribution of *C* significantly impacts FoS and probabilities of failure. For semi-infinite distributions, right-censoring introduces a bias that artificially amplifies the weight of the distribution near the maximum bound. This amplification can lead to a decrease in the mean FoS and an increase in its standard deviation compared to a bounded interval distribution (RAFF). Despite a conventional belief suggesting negligible errors from right-censoring in semi-infinite distributions near the maximum bound, these errors can be noteworthy, especially for very highly heterogeneous cohesions resulting in a low FoS. In a reliability study, it is therefore important to test multiple distributions that represent the significant data in the study, thereby ensuring more robust results for both the factor of safety and the probability of failure.

This new bounded distribution (RAFF) has been specifically crafted for addressing slope stability concerns in mining deposits. Its applicability extends broadly to various scenarios involving the reliability assessment of heterogeneous materials, encompassing applications such as compaction calculations in similar operations.

5 Appendices

A) Statistical parameters of 4 non censored semi-infinite continuous distributions.

distribution parameters	probability density function (pdf)	cumulative density function (CDF=*p*) and quantile (*x*)	mean, standard deviation
N (μ,σ)	$\frac{1}{\sigma\sqrt{2\pi}}\mathrm{e}^{-\frac{1}{2}\left(\frac{x-\mu}{\sigma}\right)^2}$	$p=\frac{1}{2}\left(1+\mathrm{Erf}\left(\frac{x-\mu}{\sqrt{2}\sigma}\right)\right)$ $x=\mu+\sqrt{2}\sigma\xi$	μ, σ

LN (μ_{LN}, σ_{LN})	$\frac{1}{\sigma_{LN} x\sqrt{2\pi}} e^{-\frac{1}{2}\left(\frac{\ln x-\mu_{LN}}{\sigma_{LN}}\right)^2}$	$p=\frac{1}{2}\left(1+\mathrm{Erf}\left(\frac{\ln x-\mu_{LN}}{\sqrt{2}\sigma_{LN}}\right)\right)$ $x=\exp\left(\mu_{LN}+\sqrt{2}\sigma_{LN}\xi\right)$ $\boxed{\xi=\mathrm{Erf}^{-1}(2p-1)}$	$\mu=e^{\mu_{LN}+\frac{\sigma_{LN}^2}{2}}$ $\sigma=\mu\sqrt{e^{\sigma_{LN}^2}-1}$ $\mu_{LN}=\ln\left(\frac{\mu^2}{\sqrt{\mu^2+\sigma^2}}\right)$ $\sigma_{LN}=\sqrt{\ln\left(1+\frac{\sigma^2}{\mu^2}\right)}$
BS (β,γ) $c=\frac{\sigma}{\mu}<\sqrt{5}$	$\frac{\sqrt{\frac{x}{\beta}}+\sqrt{\frac{\beta}{x}}}{2\sqrt{2\pi}\gamma x} e^{-\frac{\frac{x}{\beta}+\frac{\beta}{x}-2}{2\gamma^2}}$	$x=\beta\left(1+z\left(z-\sqrt{2+z^2}\right)\right)\quad p\le\frac{1}{2}$ $x=\beta\left(1+z\left(z+\sqrt{2+z^2}\right)\right)\quad p\ge\frac{1}{2}$ $z=\gamma\xi$	$\mu=\frac{\beta}{2}\left(2+\gamma^2\right)$ $\sigma=\frac{\beta}{2}\gamma\sqrt{4+5\gamma^2}$ $\beta=\frac{\mu}{3}\left(4-\sqrt{3c^2+1}\right)$ $\gamma=\sqrt{\frac{2\left(c^2-1+\sqrt{3c^2+1}\right)}{5-c^2}}$
GIG (μ_G, σ_G, θ) $c_G=\frac{\sigma_G}{\mu_G}$	$\frac{\left(\frac{x}{\mu_G}\right)^{\theta} e^{-\frac{\mu_G\left(x^2+\mu_G^2\right)}{2x\sigma_G^2}}}{2xK_{\theta}\left(c_G^{-2}\right)}$	no closed form solution	$\mu=\mu_G\frac{K_{\theta+1}\left(c_G^{-2}\right)}{K_{\theta}\left(c_G^{-2}\right)}$ $\sigma=\mu_G\sqrt{\frac{K_{\theta+2}\left(c_G^{-2}\right)}{K_{\theta}\left(c_G^{-2}\right)}-\frac{K_{\theta+1}^2\left(c_G^{-2}\right)}{K_{\theta}^2\left(c_G^{-2}\right)}}$

Table A.1: Statistical parameters of 4 non-censored semi-infinite continuous distributions (K_θ is the modified Bessel function of 2nd kind, and Erf is the error function)

B) Formulae for the censored distributions

- Interval-censored mean and standard deviation of the normal distribution: $\mathrm{N}(\mu_r, \sigma_r)$

$$\mu_C=\frac{\sigma_r}{\sqrt{2\pi}}\left(e^{-\frac{\mu_r^2}{2\sigma_r^2}}-e^{-\left(\frac{C_{\max}-\mu_r}{\sqrt{2}\sigma_r}\right)^2}\right)+\frac{\mu_r}{2}\rho+\frac{C_{\max}}{2}\rho_c \tag{B.1}$$

$$\sigma_C=\sqrt{\frac{1}{2}\left(\left(e^{-\frac{\mu_r^2}{2\sigma_r^2}}\mu_r-\left(C_{\max}+\mu_r\right)e^{-\left(\frac{C_{\max}-\mu_r}{\sqrt{2}\sigma_r}\right)^2}\right)\sqrt{\frac{2}{\pi}}\sigma_r+\left(\sigma_r^2+\mu_r^2\right)\rho+C_{\max}^2\rho_c\right)-\mu_C^2} \tag{B.2}$$

Where $\rho=\mathrm{Erf}\left(\frac{C_{\max}-\mu_r}{\sqrt{2}\sigma_r}\right)+\mathrm{Erf}\left(\frac{\mu_r}{\sqrt{2}\sigma_r}\right)$; $\rho_c=\mathrm{Erfc}\left(\frac{C_{\max}-\mu_r}{\sqrt{2}\sigma_r}\right)$

- Right-censored mean and standard deviation of the log-normal distribution: $\mathrm{LN}(\mu_r, \sigma_r)$

$$\mu_C=\frac{1}{2}\left(e^{\frac{\sigma_{LN}^2}{2}+\mu_{LN}}\,\mathrm{Erfc}\left(\frac{\sigma_{LN}^2+\mu_{LN}-\ln C_{\max}}{\sqrt{2}\sigma_{LN}}\right)+C_{\max}\left(1+\mathrm{Erf}\left(\frac{\mu_{LN}-\ln C_{\max}}{\sqrt{2}\sigma_{LN}}\right)\right)\right) \tag{B.3}$$

$$\sigma_{LN}=\sqrt{\frac{1}{2}\left(e^{2\left(\sigma_{LN}^2+\mu_{LN}\right)}\operatorname{Erfc}\left(\frac{2\sigma_{LN}^2+\mu_{LN}-\ln C_{\max}}{\sqrt{2}\sigma_{LN}}\right)+C_{\max}^2\left(1+\operatorname{Erf}\left(\frac{\mu_{LN}-\ln C_{\max}}{\sqrt{2}\sigma_{LN}}\right)\right)\right)-\mu_{LN}^2} \quad \text{(B.4)}$$

Where $\mu_{LN}=\ln\left(\frac{\mu_r^2}{\sqrt{\mu_r^2+\sigma_r^2}}\right)$ and $\sigma_{LN}=\sqrt{\ln\left(1+\frac{\sigma_r^2}{\mu_r^2}\right)}$

- Right-censored mean and standard deviation of the BS distribution (using parameters β_r, γ_r)

$$\mu_r=\frac{1}{4}\left(2C_{\max}-2e^{-\left(\frac{C_{\max}-\beta_r}{\lambda}\right)^2}\frac{\lambda}{\sqrt{\pi}}+\kappa+\left(2C_{\max}-\kappa\right)\rho-e^{\frac{2}{\gamma_r^2}}\beta_r\gamma_r^2\rho_c\right) \quad \text{(B.5)}$$

$$\sigma_r=\sqrt{\frac{1}{4}\left(2C_{\max}{}^2-2e^{-\left(\frac{C_{\max}-\beta_r}{\lambda}\right)^2}\frac{\lambda}{\sqrt{\pi}}\left(C_{\max}+\beta_r\left(1+3\gamma_r^2\right)\right)+\eta+\left(2C_{\max}{}^2-\eta\right)\rho-e^{\frac{2}{\gamma_r^2}}\beta_r^2\gamma_r^2\left(3\gamma_r^2-2\right)\rho_c\right)-\mu_r^2} \quad \text{(B.6)}$$

Where $c_r=\frac{\sigma_r}{\mu_r}$; $\beta_r=\frac{\mu_r}{3}\left(4-\sqrt{3c_r^2+1}\right)$; $\gamma_r=\sqrt{\frac{2\left(c_r^2-1+\sqrt{3c_r^2+1}\right)}{5-c_r^2}}$; $\lambda=\gamma_r\sqrt{2C_{\max}\beta_r}$; $\kappa=\beta_r\left(2+\gamma_r^2\right)$;

$\eta=\beta_r^2\left(2+4\gamma_r^2+3\gamma_r^4\right)$; $\rho=\operatorname{Erf}\left(\frac{\beta_r-C_{\max}}{\lambda}\right)$; $\rho_c=\operatorname{Erfc}\left(\frac{\beta_r+C_{\max}}{\lambda}\right)$

- Right-censored mean and standard deviation of the GIG distribution (μ_r, σ_r, θ_r)

The integrals below do not have analytical solutions and must therefore be evaluated numerically.

$$\tilde{\mu}=\int_{C_{\min}}^{C_{\max}}\frac{x^{\theta_r}e^{-\frac{\mu_r\left(x^2+\mu_r^2\right)}{2x\sigma_r^2}}}{2\mu_r^{\theta_r}K_\theta\left(c_r^{-2}\right)}dx+C_{\max}\int_{C_{\max}}^{\infty}\frac{x^{\theta_r-1}e^{-\frac{\mu_r\left(x^2+\mu_r^2\right)}{2x\sigma_r^2}}}{2\mu_r^{\theta_r}K_{\theta_r}\left(c_r^{-2}\right)}dx \quad \text{(B.7)}$$

$$\tilde{\sigma}=\sqrt{\int_{C_{\min}}^{C_{\max}}\frac{e^{-\frac{\mu_r\left(x^2+\mu_r^2\right)}{2x\sigma_r^2}}}{2\mu_r^{\theta_r}K_{\theta_r}\left(c_r^{-2}\right)}dx+C_{\max}^2\int_{C_{\max}}^{\infty}\frac{x^{\theta_r-1}e^{-\frac{\mu_r\left(x^2+\mu_r^2\right)}{2x\sigma_r^2}}}{2\mu_r^{\theta_r}K_{\theta_r}\left(c_r^{-2}\right)}dx-\tilde{\mu}^2} \quad \text{(B.8)}$$

Funding: This work has received funding from the European Union's Research Fund for Coal and Steel (RFCS). under the project "Risk Assessment of final Pits during Flooding (RAFF)". No 847299.

6 References

[1] D.Y.A. Massih, A.H. Soubra, Effet de la variabilité spatiale du sol dans l'étude du comportement des fondations superficielles filantes, Rev. Fr. Geotech. 130 (2010) 41-51 (in French). https://www.geotech-fr.org/sites/default/files/rfg/numero/RFG_2010_N_130.pdf.

[2] M.A. Hicks, J.D. Nuttall, J. Chen, Influence of heterogeneity on 3D slope reliability and failure consequence, Comput. Geotech. 61 (2014) 198-208. https://doi.org/10.1016/j.compgeo.2014.05.004.

[3] D.V. Griffiths, G.A. Fenton, Probabilistic Slope Stability Analysis by Finite Elements, J. Geotech. Geoenviron. Eng. 130 (5) (2004) 507-518. https://doi.org/10.1061/(ASCE)1090-0241(2004)130:5(507).

[4] J.M. Duncan, Factors of safety and reliability in geotechnical engineering, J. Geotech. Geoenviron. Eng. 126 (4) (2000) 307-316. https://doi.org/10.1061/(ASCE)1090-0241(2000)126:4(307).
[5] K. Farah, M. Ltifi, T. Abichou, H. Hassis, Comparison of some probabilistic methods for analyzing slope stability problem, Int. J. Civ. Eng. 12 (2013) 264-268. http://www.iust.ac.ir/ijce/article-1-871-en.pdf (accessed 27 February 2024)
[6] M. Matsuo, K. Kuroda, Probabilistic approach to design of embankments, Soils Found. 14 (2) (1974) 1-17. https://doi.org/10.3208/sandf1972.14.2_1.
[7] A.H.S. Ang, W.H. Tang, Probability concepts in engineering planning and design, Vol. 1, Basic principles, John Wiley, New York, 1975.
[8] E.E. Alonso, Risk analysis of slopes and its application to slopes in Canadian sensitive clays, Géotechnique 26 (3) (1976) 453-472. https://doi.org/10.1680/geot.1976.26.3.453.
[9] E.H. Vanmarcke, Reliability of earth slopes, J. Geotech. Eng., ASCE 103 (11) (1977) 1247-1265. https://doi.org/10.1061/AJGEB6.0000518.
[10] H.E. Ramly, N.R. Morgenstern, D.M. Cruden, Probabilistic slope stability analysis for practice, Can. Geotech. J. 39 (3) (2002) 665-683. https://doi.org/10.1139/t02-034.
[11] O. Ditlevsen, H.O. Madsen, Structural reliability methods, John Wiley & Sons, Chichester,1996. https://orbit.dtu.dk/en/publications/structural-reliability-methods (accessed 27 February 2024)
[12] A.H.S. Ang, W.H. Tang, Probability concepts in engineering planning and design, Vol. 2, Basic principles, John Wiley, New York, 1984.
[13] I.E. Zevgolis, A.V. Deliveris, N.C. Koukouzas, Probabilistic design optimization and simplified geotechnical risk analysis for large open pit excavations, Comput. Geotech. 103 (2018) 153-164. https://doi.org/10.1016/j.compgeo.2018.07.024.
[14] C. Obregon, H.Mitri, Probabilistic approach for open pit bench slope stability analysis – A mine case study, Int. J. Min. Sci. Tech. 29 (4) (2019) 629-640. https://doi.org/10.1016/j.ijmst.2019.06.017.
[15] D.Q. Li, Y.F. Chen, W.B. Lu, C.B. Zhou, Stochastic response surface method for reliability analysis of rock slopes involving correlated non-normal variables, Comput. Geotech. 38 (1) (2011) 58-68. https://doi.org/10.1016/j.compgeo.2010.10.006.
[16] V. Merrien-Soukatchoff, T. Korini, A. Thoraval, Use of an Integrated Discrete Fracture Network Code for Stochastic Stability Analyses of Fractured Rock Masses, Rock Mech. Rock Eng. 45 (2012) 159-181. https://doi.org/10.1007/s00603-011-0136-7.
[17] M.L. Napoli, M. Barbero, E. Ravera, C. Scavia, A stochastic approach to slope stability analysis in bimrocks, Int. J. Rock Mech. Min. Sci. 101 (2018) 41-49. https://doi.org/10.1016/j.ijrmms.2017.11.009.
[18] D.G. Kendall, Foundations of a theory of random sets, in: E.F Harding, D.G. Kendall (Eds.), Stochastic geometry, Wiley, New York, 1974, pp. 322-376.
[19] D.V. Griffiths, J. Huang, G.A. Fenton, Influence of spatial variability on slope reliability using 2-D random fields, J. Geotech. Geoenviron. Eng. 135 (10) (2009) 1367-1378 (technical papers). https://doi.org/10.1061/(ASCE)GT.1943-5606.0000099.
[20] R.G. Ghanem, P.D. Spanos, Stochastic finite element: a spectral approach, Springer-Verlag, New York, 1991. http://dx.doi.org/10.1007/978-1-4612-3094-6.
[21] A.M. Afrapoli, M. Osanloo, Determination and stability analysis of ultimate open-pit slope under geomechanical uncertainty, Int. J. Min. Sci. Tech. 24 (1) (2014) 105-110. https://doi.org/10.1016/j.ijmst.2013.12.018.
[22] B. Pandit, G. Tiwari, G.M. Latha, G.L.S. Babu, Stability Analysis of a Large Gold Mine Open?Pit Slope Using Advanced Probabilistic Method, Rock Mech. Rock Eng. 51 (2018) 2153-2174. https://doi.org/10.1007/s00603-018-1465-6.
[23] X. Li, Q.L. Liao, J.M. He, In situ tests and a stochastic structural model of rock and soil aggregate in the three Gorges Reservoir area, China, Int. J. Rock Mech. Min. Sci. 41 (Suppl. 1) (2004) 702-707. https://doi.org/10.1016/j.ijrmms.2004.03.122.

[24] H. Shen, S.M. Abbas, Rock slope reliability analysis based on distinct element method and random set theory, Int. J. Rock Mech. Min. Sci. 61 (2013) 15-22. https://doi.org/10.1016/j.ijrmms.2004.03.122.
[25] S. Fityus, G. Hancock, T. Wells, Geotechnical characterization of coal mine spoil. Aust. Geomech. J. 43 (3) (2008) 13-22. https://nova.newcastle.edu.au/vital/access/manager/Repository/uon:4607 (accessed 27 February 2024)
[26] S. Sharma, I. Roy, Slope failure of waste rock dump at Jayant opencast mine, India: a case study, Int. J. Appl. Eng. Res. 10 (13) (2015) 33006-33012. https://www.bitmesra.ac.in/UploadedDocuments/admnaac/files/3_4_5_CEE_File%202_Evidence.pdf (accessed 27 February 2024)
[27] R.M. Bishwal, P. Sen, M. Jawed, Characterization of Shear Strength Properties of Spoil Dump Based on their Constituent Material, Int. J. App. Eng. Res. 12 (19) (2017) 8590-8594. https://www.ripublication.com/ijaer17/ijaerv12n19_80.pdf (accessed 27 February 2024)
[28] I.E. Zevgolis, 2018. Geotechnical characterization of mining rock waste dumps in central Evia, Greece. Environ. Earth Sci. 77, 566. https://doi.org/10.1007/s12665-018-7743-5.
[29] C. Oggeri, R. Vinai, 2020. Characterisation of geomaterials and non-conventional waste streams for their reuse as engineered materials, in: Proc. 4th European Conference on Saturated Soils (E-UNSAT 2020). E3S Web of Conferences. 195, 06002. https://doi.org/10.1051/e3sconf/202019506002.
[30] I.E. Zevgolis, A. Theocharis, A.V. Delivers, N.C. Koukouzas, C. Roumpos, A.M. Marshall, Geotechnical characterization of fine-grained spoil material from surface coal mines, J. Geotech. Environ. Eng. 147 (7) (2021) 04021050. https://doi.org/10.1061/%28ASCE%29GT.1943-5606.0002550.
[31] I. McLean, Lessons from the Aberfan disaster and its aftermath. Brit. Acad. Rev. 12 (2009) 49-52. https://www.thebritishacademy.ac.uk/documents/769/16-mclean.pdf (accessed 27 February 2024)
[32] E. Steiakakis, K. Kavouridis, D. Monopolis, Large scale failure of the external waste dump at the “South Field” lignite mine, Northern Greece. Eng. Geol. 104 (3-4) (2009) 269-279. https://doi.org/10.1016/j.enggeo.2008.11.008.
[33] I.E. Zevgolis, A.V. Deliveris, N.C. Koukouzas, Slope failure incidents and other stability concerns in surface lignite mines in Greece. J. Sustain. Min. 18 (4) (2019) 182-197. https://doi.org/10.1016/j.jsm.2019.07.001.
[34] I. Kadar, L. Nagy, The examination of different soil parameters, coefficient of variation values and types of distribution, Proceedings of the 6th international Young Geotechnical Engineers’ Conference, iYGEC6, Seoul, South Korea, 16-17 September 2017. https://www.issmge.org/uploads/publications/48/49/soil-behaviors-characterization-iii-2.pdf.
[35] M.S. Masoudian, I.E. Zevgolis, A.V. Deliveris, A. Marshall, C. Heron, N.C. Koukouzas, 2019. Stability and characterisation of spoil heaps in European surface lignite mines: a state-of-the-art review in light of new data. Environ. Earth Sci. 78, 505. https://doi.org/10.1007/s12665-019-8506-7.
[36] S. Olesiak, Influence of the heterogeneity of a dump soil on the assessment of its selected properties, Stud. Geotech. Mech. 42 (3) (2020) 263-275. https://doi.org/10.2478/sgem-2020-0001.
[37] J. Pieczynska-Koz?owska, I. Baginska, M. Kawa, 2021. The Identification of the Uncertainty in Soil Strength Parameters Based on CPTu Measurements and Random Fields. Sensors. 21, 5393. https://doi.org/10.3390/s21165393.
[38] ISSMGE-TC304, State-of-the-art review of inherent variability and uncertainty in geotechnical properties and models, International Society of Soil Mechanics and Geotechnical Engineering (ISSMGE) - Technical Committee TC304 ‘Engineering Practice of Risk Assessment and Management’, 02 March 2021. https://doi.org/10.53243/R0001.

[39] B.C. Arnold, R.A. Groeneveld, Measuring skewness with respect to the mode, Am. Stat. 49 (1) (1995) 34-38. https://doi.org/10.1080/00031305.1995.10476109.
[40] H. Albrecht, T. Hamacher, R.P. Hofmann, T. Kirchhoff, R. Mankel, A. Nau, … & Argus Collaboration, Measurement of the polarization in the decay B ? J/?K*, Physics Letters B. 340 (3) (1994) 217-220. https://doi.org/10.1016/0370-2693(94)01302-0.
[41] G. Nemes, A.B.O. Daalhuis, Asymptotic expansions for the incomplete gamma function in the transition regions, Math. Comput. 88 (2019) 1805-1827. https://doi.org/10.1090/mcom/3391.
[42] G.E.P. Box, M.E. Muller, A Note on the Generation of Random Normal Deviates, Ann. Math. Stat. 29 (2) (1958) 610-611. https://doi.org/10.1214/aoms/1177706645.
[43] S. Winitzki, Uniform approximations for transcendental functions, in: V. Kumar et al. (Eds.), Proceedings of the International Conference on Computational Science and Its Applications, ICCSA 2003, 18-21 May 2003, Montreal, Canada, Lecture Notes 2667, Springer-Verlag, Berlin Heidelberg, 2003, pp. 780-789. https://doi.org/10.1007/3-540-44839-X_82.
[44] J.R. Michael, W.R. Schucany, R.W. Haas, Generating Random Variates Using Transformations with Multiple Roots, Am. Stat. 30 (2) (1976) 88-90. https://doi.org/10.1080/00031305.1976.10479147.
[45] A.C. Atkinson, The simulation of generalized inverse Gaussian and hyperbolic random variables, SIAM J. Sci. Comput. 3 (4) (1982) 502-515. https://doi.org/10.1137/0903033.
[46] S. Zhang, Transition law-based simulation of generalized inverse Gaussian Ornstein-Uhlenbeck processes, Methodol. Comput. Appl. Probab. 13 (2011) 619-656. https://doi.org/10.1007/s11009-010-9179-6.
[47] W. Hormann, J. Leydold, Generating generalized inverse Gaussian random variates, Stat. Comput. 24 (2014) 547-557. https://doi.org/10.1007/s11222-013-9387-3.
[48] L. Devroye, Random variate generation for the generalized inverse Gaussian distribution, Stat. Comput. 24 (2014) 239-246. https://doi.org/10.1007/s11222-012-9367-z.
[49] P. Lumb, Safety factors and probability distribution of soil strength, Can. Geotech. J. 7 (3) (1970) 225-242. https://doi.org/10.1139/t70-032.
[50] V. Renaud, M. Al Heib, J. Burda, 2022. 3D large scale numerical model of open-pit lake slope stability - case study of Lake Most. B. Eng. Geol. Environ. 81, 282. https://doi.org/10.1007/s10064-022-02771-3.
[51] W. Gibson, Probabilistic methods for slope analysis and design, Aust. Geomech. J. 46 (3) (2011) 29-39. https://australiangeomechanics.org/papers/probabilistic-methods-for-slope-analysis-and-design/ (accessed 27 February 2024)
[52] Itasca Consulting Group Inc., Fast Lagrangian Analysis of Continua in Three Dimensions (FLAC3D) v7.0 (Version 7.0), Minneapolis: Itasca, 2019. https://docs.itascacg.com/flac3d700/flac3d/docproject/source/flac3dhome.html (accessed 27 February 2024)